Journal of

Applied and Computational Mechanics

Shahid Chamran
University of Ahvaz

Research Paper

Bifurcation of Fiber-Reinforced Cylindrical Membranes under Extension, Inflation, and Swelling

Heiko Topol[1], Murtadha J. Al-Chlaihawi[2,3], Hasan Demirkoparan[4], José Merodio[5]

[1] Institute of General Mechanics, RWTH Aachen University, Eilfschornsteinstr. 18, 52062 Aachen, Germany, Email: topol@iam.rwth-aachen.de

[2] Civil Engineering Department, University of Al-Qadisiyah, 58001 Al-Qadisiyah, Iraq

[3] Department of Continuum Mechanics and Structures, Universidad Politecnica de Madrid, Spain, Email: murtadha.hussein@alumnos.upm.es

[4] Carnegie Mellon University in Qatar, P.O. Box 24866, Doha, Qatar, Email: hasand@qatar.cmu.edu

[5] Departamento de Matemtica Aplicada a las TIC, ETS de Ingeniera de Sistemas Informticos, Universidad Politecnica de Madrid, Spain, Email: merodioj@gmail.com

Abstract. We analyze bifurcation for a cylindrical membrane capable of swelling subjected to combined axial loading and internal pressure. The material is conceptualized as an isotropic and absorbent matrix (it can swell when it is exposed to some swelling agent, for instance) containing nonabsorbing fibers. More in particular, fibers are symmetrically arranged in two helically distributed families which are (also) mechanically equivalent. Arterial wall tissue has been modeled using this theoretical framework. The matrix of the membrane is taken to be a swellable neo-Hookean material. The swollen membrane is then inflated and axially stretched so that the circular cylindrical geometry is initially preserved. Nevertheless, prismatic, bulging, and bending (composite) bifurcation conditions are analyzed. It is shown that for membranes with and without fibers, prismatic bifurcation does not play a major role. On the other hand, bending and bulging are feasible for fiber-reinforced membranes. Results capture the onset of bifurcation configurations corresponding to bending and bulging and highlight possible coupling during postbifurcation as it might occur, for example, in the formation and development of an abdominal aortic aneurysm.

Keywords: Bulging bifurcation; bending bifurcation; prismatic bifurcation; swelling; fibers; hyperelasticity.

1. Introduction

Abdominal aortic aneurysms are reported to be responsible for 1-2% of all deaths in industrialized countries [1]. In many cases, this pathology remains undiagnosed until rupture occurs and it has a mortality rate that is greater than 80% [2]. This has been a main motivation for researchers in different areas to develop models to capture and to understand the formation, development and, rupture of aneurysms.

There are many factors that play an important role in the formation of such pathological dilatations of arteries, among them, one can include geometry, mechanical properties as well as numerous biochemical processes. Different research works study the formation and development of aneurysms from a mechanical point of view as a mechanism related to various bifurcation and post-bifurcation behaviors of extended and pressurized soft hollow cylinders. Indeed, the formation of instabilities depends on the material as well as on both the internal pressure of the cylinder and the axial loading (stretch), which has been shown in different theoretical and experimental works during the last decades [3–17].

This article focuses on three bifurcation modes that may occur in the context of axially loaded and inflated anisotropic and volume changing cylinders, namely bulging bifurcation, prismatic bifurcation, and bending (composite) bifurcation. In the context of hyperelastic materials, the conditions for the existence of such instability modes have been derived, for example, by [9]. Bulging bifurcation has been investigated in various contexts [9, 10], but the same attention has not been paid to the other two bifurcation modes. Very recently it has been recognized that coupling of different bifurcation modes during postbifurcation is important to capture the development of abdominal aortic aneurysms [15, 16]. With this in mind, we pay attention to the onset of different bifurcation modes for a swellable material reinforced with two preferred directions. Prismatic bifurcation analyses can be found for both cylindrical membranes [5] and for thick-walled tubes [18]. Similarly, different bifurcation modes have been studied in the modeling of arterial tissue that is affected by Marfan's syndrome, which is a connective tissue disorder [8, 19]. Residual stresses have an influence on the bifurcation of extended and inflated cylinders [20, 21]. In particular, Haughton and Merodio [22] presented a computational bending and bulging bifurcation analysis for residually stressed hyperelastic tubes under combined inflation and extension to model aneurysms in arterial tissue.
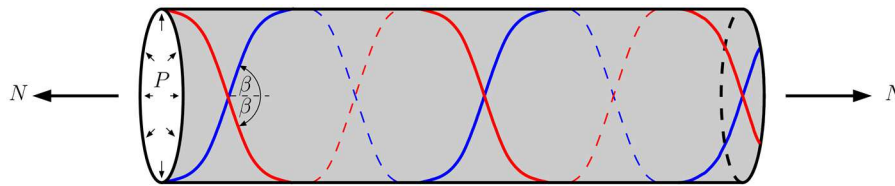
Fig. 1. A cylinder that is subjected to both an inflation pressure P and an axial load N. The material consists of a swellable isotropic ground substance material that is reinforced by two families of fibers.

Many works on bifurcation consider a volume-preserving context, whereas different factors such as edema, mechanical trauma, and inflammations [23–25] lead to swelling of biological materials. Swelling may not only increase the volume, but also the stiffness of the swollen material. Both, the change in the geometry and in the mechanical properties have an impact on bifurcation, i.e., swelling may stabilize the cylinder against the occurrence of one particular bifurcation mode while it may trigger the formation of other bifurcation modes. In hyperelastic materials, swelling has been taken into account in different modeling works for isotropic [26, 27] and anisotropic materials [28]. It has been shown that collagen remodeling processes may be driven by changes in the tissue volume (see [29,30]). Our previous works have shown that changes in the material volume may have a beneficial effect with respect to preventing bulging bifurcation [31, 32]. [33] then explore the role of swelling on the formation of instability modes, namely prismatic and bending bifurcation in some fibrous cylinders, which motivates this work. For most of the works that invoke swelling to study bifurcation of inflated and extended cylinders the material stiffness is taken to be independent of swelling [31–33]. Here we also pay attention to that aspect. In addition, many of the works on the formation of an instability have their focus on the individual analysis of bifurcation modes. This work compares the occurrence of bulging, prismatic, and bending bifurcation in fibrous and swelling cylinders with the aim to establish possible coupling of different modes during post-bifurcation.

This article is structured as follows: Section 2 introduces the main kinematics of the problem at hand as well as the material models. Section 3 discusses the bifurcation modes which in Section 4 are examined for the material models under consideration. More in particular, Section 4 studied bifurcation for an isotropic cylinder (without fibers) based on the assumption that the material stiffness is independent from swelling effects. On the other hand, in Section 5, bifurcation is studied for a fibrous material in which the mechanical properties of the ground substance are negligible. Finally, Section 6 illustrates the impact of swelling-dependent stiffness changes in a ground substance with embedded fibers on bifurcation. The last section, Section 7, concludes the article with a discussion of the results and a brief outlook.

2. Kinematics and Mechanical Behavior of the Cylindrical Membrane

In a reference (unloaded) configuration Ω_r, an undeformed and hollow cylinder with inner radius A, outer radius B, and length L is described in terms of a cylindrical coordinate system (R, Θ, Z) with unit vectors (E_R, E_θ, E_Z), respectively, as

$$A \le R \le B, \quad 0 \le \Theta \le 2\pi, \quad -L/2 \le Z \le L/2. \tag{1}$$

Any point of this cylinder can be given by the position vector

$$X = R E_R(\Theta) + Z E_Z. \tag{2}$$

The cylinder is subject to both an inflation pressure P and an axial load N so that it preserves the shape of a circular tube (see Fig. 1). In the deformed configuration Ω, the cylinder is described in terms of a cylindrical coordinate system (r, θ, z) with unit vectors (e_r, e_θ, e_z), respectively, as

$$a \le r \le b, \quad 0 \le \theta \le 2\pi, \quad -l/2 \le z \le l/2, \tag{3}$$

and any point of this cylinder can be given by the position vector

$$x = r e_r(\theta) + z e_z. \tag{4}$$

The material is capable of swelling, which is described by the ratio of the swollen material volume to the unswollen material volume by means of the parameter v. At each time during the swelling process, the material is taken to be incompressible. Such an idealization is reasonable in arterial tissue, for instance, due to the high water content of the tissue. Our considerations focus on uniform swelling of the material without local variations. For such a deformation of the cylinder, the deformation gradient has the form

$$F = \mathrm{diag}(\lambda_r, \lambda_\theta, \lambda_z), \tag{5}$$

where λ_r is the radial stretch, $\lambda_\theta = r/R \equiv \lambda$ is the circumferential (azimuthal) stretch and $\lambda_z = l/L$ is the axial stretch. The condition $\det F = v$ for the swollen material allows to write the radial stretch as $\lambda_r = v\lambda^{-1}\lambda_z^{-1}$.

For such a swelling solid the relation between the Cauchy stress tensor σ and the deformation can be expressed via

$$\sigma = -pI + \frac{1}{v}\frac{\partial W}{\partial F} F^T, \tag{6}$$

where I is the second order identity tensor and p is a scalar that results from the (incompressibility) constraint. The Cauchy stress tensor satisfies the condition $\mathrm{div}\,\sigma = 0$ in the absence of body forces. There exist numerous material models that have been derived to describe the mechanical behavior of fibrous soft tissue [37]. In these models, the material is treated in a homogenized sense so that each material point contains both ground substance and fiber constituents. We consider orthotropic materials with two preferred directions which are mechanically equivalent and are symmetrically disposed. The mechanical behavior of such materials is often defined in terms of a strain energy density function which may be decomposed into a contribution W_m of the ground substance material and into a contribution W_f of the embedded fibers, i.e.

$$W = W_m + W_f. \tag{7}$$

Here, the mechanical behavior of the isotropic ground substance is described by the Treloar model [38],

$$W_m(I_1, v) = \frac{\mu v^{q-2/3}}{2}(I_1 - 3v^{2/3}), \tag{8}$$

where

$$I_1 = \text{tr}\,\boldsymbol{C} = \frac{v^2}{\lambda^2 \lambda_z^2} + \lambda^2 + \lambda_z^2, \tag{9}$$

is the first invariant of the right Cauchy-Green deformation tensor $\boldsymbol{C} = \boldsymbol{F}^T \boldsymbol{F}$, the parameter v accounts for swelling, and μ is the shear modulus for an unswollen material. The term $\mu v^{q-2/3}$ can be seen as a swelling-dependent shear modulus, in which the parameter q quantifies the change of the ground substance stiffness with swelling. If $q = 2/3$, then the ground substance is swelling-independent. The matrix stiffness decreases with swelling if $q < 2/3$, and it increases with swelling if $q > 2/3$. The model (8) is a generalization of the incompressible neo-Hookean model that accounts for swelling, and it has found its application in different modeling works [32, 33, 39, 40]. Despite their relatively simple form, neo-Hookean type models are used to model arterial tissue. For example, it has been shown that such types of models can (sufficiently) describe the mechanical behavior of arterial elastin [41]. Furthermore, the neo-Hookean form can be understood as a particular case of many constitutive equations used in the modeling of soft tissue constituents. For instance, Mooney-Rivlin materials are a generalization of the neo-Hookean model, and swelling of Mooney-Rivlin type models have been studied to capture bulging bifurcation in [35]. Different works that account for swelling in the examination of bifurcation neglect the role of the parameter q in (8), which, in addition, motivates the present work.

With respect to the fibers, it is assumed that they are embedded in the ground substance and are incapable of swelling. In the membrane, fibers are grouped in two (fiber) families with equal mechanical properties. The initial (undeformed) orientation of each fiber family is given by a unit vector in the reference configuration Ω_r. Both families are symmetrically disposed with respect to the axial direction. It follows that the two unit vectors in Ω_r giving the directions of the two families of fibers can be written as

$$\boldsymbol{M}_1 = cos\beta \boldsymbol{E_Z} + sin\beta \boldsymbol{E_\theta}, \tag{10a}$$

$$\boldsymbol{M}_2 = cos\beta \boldsymbol{E_Z} - sin\beta \boldsymbol{E_\theta}, \tag{10b}$$

in which β, the fiber winding angle, gives the orientation of each fiber family with respect to the axial direction of the membrane. The mechanical behavior of the first fiber family is described in terms of the invariant I_4, and the mechanical behavior of the second fiber family is described in terms of the invariant I_6 (which are sometimes referred to as "pseudo-invariants"), which are

$$I_4 = \boldsymbol{C}:\boldsymbol{M}_1 \otimes \boldsymbol{M}_1 = \lambda_z^2 cos^2\beta + \lambda^2 sin^2\beta, \tag{11a}$$

$$I_6 = \boldsymbol{C}:\boldsymbol{M}_2 \otimes \boldsymbol{M}_2 = \lambda_z^2 cos^2\beta + \lambda^2 sin^2\beta. \tag{11b}$$

Under the circumstances at hand, I_4 and I_6 are equal. These invariants are interpreted as the squared magnitude of the fiber stretch. The fibers bear tension, whereas they are taken to be incapable of carrying (fiber) compression. This means that I_4 and I_6 can just take values that are equal to one or greater than one. While in this article the elastic fiber behavior is described in terms of the invariants I_4 and I_6, higher invariants may be introduced to account for different mechanical properties of the fibers and their interplay. We should also note that in this work we assume that the fibers are in a perfect parallel arrangement within each fiber family. Modifications of I_4 and I_6 and higher invariants that account for fiber dispersion are discussed in [42]. In addition, in our modeling, all constituents are taken to share a common natural configuration, and, for convenience, this configuration is taken to be the reference configuration. Topol et al. [43] consider bulging bifurcation in a pressurized cylinder, in which the natural configuration of the constituents may differ.

We further consider a strain energy density for the fibers in the form of an exponential function as

$$W_f(I_4, I_6) = \frac{k_1}{2\bar{k}_1} \sum_{i=4,6} \left[e^{\bar{k}_1(I_i-1)^2} - 1 \right], \tag{12}$$

where k_1 is a stiffness parameter and $\bar{k}_1$ can be regarded as a sensitivity parameter. These strain energy functions in exponential form are used to model arteries [44, 45], and they are motivated by a peculiar mechanical behavior of fibers, namely, fibers are initially crimped when unloaded, then they unwind (or un-crimp) as they begin to be extended until, finally, the fibers fully bear (axial) loading as they are fully unwound [46].

Since the fiber families are mechanically equivalent and symmetrically disposed, it follows that $I_4 = I_6$, and, furthermore, that

$$\frac{k_1}{\bar{k}_1}\left[e^{\bar{k}_1(I_4-1)^2} - 1\right] = \frac{k_1}{2\bar{k}_1} \sum_{i=4,6} \left[e^{\bar{k}_1(I_i-1)^2} - 1\right], \tag{13}$$

which, in turn, allows to write the strain energy contribution (12) of the two families of fibers as

$$W_f(I_4) = \frac{k_1}{\bar{k}_1}\left[e^{\bar{k}_1(I_4-1)^2} - 1\right]. \tag{14}$$

Notice that the energy form (14) reduces to the so-called standard reinforcing model in the limit

$$\lim_{\bar{k}_1 \to 0} W_f(I_4) = k_1[I_4 - 1]^2. \tag{15}$$

In summary, the strain energy is considered to be $W(I_1, v, I_4) = W_m(I_1, v) + W_f(I_4, I_6)$. Both terms $W_m(I_1, v)$ and $W_f(I_4, I_6)$ will be analyzed independently as well as combined with regard to bifurcation. Due to the dependence of the invariants on the stretches λ and λ_z and on the swelling field we introduce the (convenient) notation $\widehat{W}(v, \lambda, \lambda_z) = W(I_1, v, I_4)$. Similarly, and accordingly, one can also write $\widehat{W}_m$ and $\widehat{W}_f$. In the next section, firstly, bifurcation modes of the cylinder are introduced in an illustrative way.

3. Bifurcation Modes in the Membrane Approximation

We consider the cylinder in the membrane approximation, in which the cylinder is taken to have the midsurface radius $R = (A + B)/2$ and the wall thickness $H = (B - A) \ll R$. The cylinder is assumed to have an infinite length $L \to \infty$ or, alternatively, $R \ll L$.

This membrane approximation permits to obtain analytical expressions for bifurcation modes. The results from these investigations give a basic understanding of bifurcation and serve as guidelines for future works dealing with thick-walled tubes, which may have to be carried out numerically.
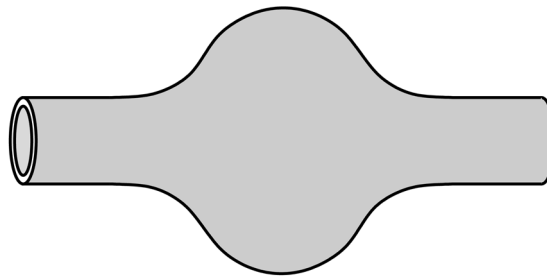
Fig. 2. Bulging bifurcation of a circular cylinder.

In this membrane approximation, the relation between the inflation pressure P, the axial normal force N, and the deformation is given by [47]

$$P = \frac{H}{R} \frac{\widehat{W}_\lambda}{\lambda \lambda_z}, \qquad N = \widehat{W}_{\lambda_z}, \tag{16}$$

where here and in the following we apply the notation $\widehat{W}_\lambda = \frac{\partial \widehat{W}}{\partial \lambda}$ in order to describe the partial derivatives of the strain energy density function $\widehat{W}$. The radial normal stresses are negligible in the membrane approximation, i.e. $\sigma_{rr} = 0$, and the components $\sigma_{\theta\theta}$ and σ_{zz} of the Cauchy stress tensor (6) can be written as

$$\sigma_{\theta\theta} = v^{-1}\lambda\widehat{W}_\lambda, \quad \sigma_{zz} = v^{-1}\lambda_z\widehat{W}_{\lambda_z}. \tag{17}$$

Note that the scalar p arising from the incompressible constraint has already been eliminated in (17).

We study three bifurcation modes, namely, bulging bifurcation, prismatic bifurcation, and bending bifurcation. Using incremental displacements, the bifurcation criterion for incompressible and anisotropic cylinders can be found in [11]. Their result is in agreement with the analysis of [6] for isotropic materials, and in recent papers, the bulging condition has been used to analyze axial propagation of bulging for thin-walled cylinders under internal pressurization [48]. To investigate the possible bifurcation, we consider incremental displacements with respect to the deformed configuration under equilibrium. In the general form, one considers [11]

$$\delta\boldsymbol{u} = \delta u_r(\theta,z)\boldsymbol{e}_r + \delta u_\theta(\theta,z)\boldsymbol{e}_\theta + \delta u_z(\theta,z)\boldsymbol{e}_z, \tag{18}$$

in which δ is the increment and $\boldsymbol{u}$ is the displacement with components (u_r, u_θ, u_z).

3.1 Bulging Bifurcation

Figure 2 depicts bulging bifurcation in a circular cylinder. The origin of this analysis goes back a while ago (see [4, 6]). Nevertheless, this topic is being studied extensively by different research groups [16, 18–20]. In order to investigate the possible bulging bifurcation mode of the cylinder, we particularize (18) and consider incremental displacements

$$\delta\boldsymbol{u} = \delta u_r(z)\boldsymbol{e}_r + \delta u_z(z)\boldsymbol{e}_z, \tag{19}$$

The bulging condition for a cylindrical membrane of radius R and length L is (see for instance [11, 34, 49])

$$f(\widehat{W}, \lambda, \lambda_z) + \left(\frac{2\pi R}{L}\right)^2 \lambda^2 \lambda_z \widehat{W}_{\lambda_z} \widehat{W}_{\lambda_z\lambda_z} = 0, \tag{20}$$

where

$$f(\widehat{W}, \lambda, \lambda_z) = \lambda_z^2 \widehat{W}_{\lambda_z\lambda_z}(\lambda^2 \widehat{W}_{\lambda_z\lambda_z} - \lambda\widehat{W}_\lambda) - (\lambda\lambda_z\widehat{W}_{\lambda\lambda_z} - \lambda\widehat{W}_\lambda)^2. \tag{21}$$

For a cylinder of infinite length, $L \to \infty$, the second term on the left side of (20) becomes negligible. Under these circumstances, for the material model at hand, the bulging condition (20) can be written as

$$f = f_{I_1} + f_{I_4} = 0, \tag{22}$$

in which the term f_{I_1} results from the mechanical behavior of the swellable neo-Hookean ground substance given in (8), while the term f_{I_4} represents the behavior of the fibers given in (14). More in particular, it is easy to obtain that,

$$f_{I_1} = \frac{[\mu v^{q-2/3}]^2(-\lambda_z^4\lambda^8 + 4\lambda_z^4\lambda^2 v^2 + 4\lambda_z^2\lambda^4 v^2 + 3v^4)}{(\lambda_z^4\lambda^4)}, \tag{23a}$$

$$f_{I_4} = [\lambda_z^2\{\lambda^2[4k_1 sin^2\beta[I_4 - 1] + 8k_1\lambda^2 sin^4\beta + 16\bar{k}_1 k_1\lambda^2 sin^4\beta[I_4 - 1]^2] - 4k_1 sin^2\beta[I_4 - 1]\}[4k_1 cos^2\beta[I_4 - 1] + 8k_1\lambda_z^2 cos^4\beta$$
$$+16\bar{k}_1 k_1\lambda_z^2 cos^4\beta[I_4 - 1]^2] - \{\lambda_z\lambda[8k_1\lambda_z\lambda cos^2\beta\ sin^2\beta + 16\bar{k}_1 k_1\lambda_z\lambda cos^2\beta\ sin^2\beta\ [I_4 - 1]^2] - 4k_1\lambda^2 sin^2\beta[I_4 - 1]\}^2 e^{2\bar{k}_1(I_4 - 1)^2}. \tag{23b}$$

The fibers do not support compression which means that $f_{I_4} = 0$ for combinations of λ_z and λ give rise to values of I_4 that are smaller than one.

Note that if $f < 0$, it follows that the membrane is unstable with regard to bulging, whereas if $f > 0$ the membrane is stable.

3.2 Prismatic Bifurcation

In a cylindrical membrane, a sufficient condition for prismatic bifurcation to exist is a turning point in the curve giving values of azimuthal stress vs azimuthal stretch. Figure 3 depicts prismatic bifurcation in an initially circular cylinder. In the prismatic bifurcation mode, the inflated cylinder bifurcates into a prismatic shape with a non-circular cross-section. In this case we particularize (18) and consider incremental displacements of the form

$$\delta\boldsymbol{u} = \delta u_r(\theta)\boldsymbol{e}_r + \delta u_\theta(\theta)\boldsymbol{e}_\theta. \tag{24}$$

Fig. 3. Prismatic bifurcation of an initially circular cylinder.
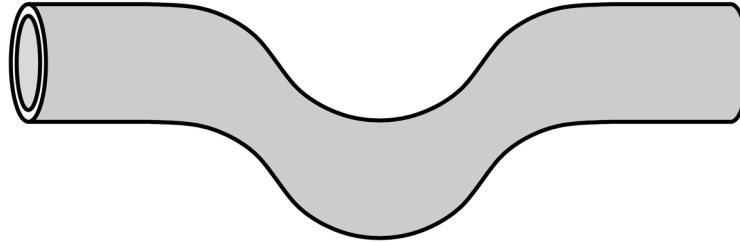

Fig. 4. Bending bifurcation of a circular cylinder.

After some manipulations, we obtain for a membrane cylinder that the bifurcation condition for the lowest (and typically most likely) mode is given by [11, 36]

$$g = \widehat{W}_{\lambda\lambda} = 0. \tag{25}$$

This condition has also been derived by [6] for thin-walled isotropic and non-swelling cylinders, while in [21] the analysis was broadened to consider thick-walled cylinders. If $g < 0$, it follows that the membrane is unstable with regard to bulging, whereas if $g > 0$ the membrane is stable.

For the material model at hand, the prismatic bifurcation condition (25) can be written as

$$g = g_{I_1} + g_{I_4} = 0, \tag{26}$$

in which, as before, the term g_{I_1} represents the mechanical behavior of the ground substance (8), while the term g_{I_4} represents the mechanical behavior of the fibers (14). From (8), (14), and (26), we obtain the terms g_{I_1} and g_{I_4} in the form

$$g_{I_1} = \frac{\mu v^{q-2/3}}{2}\left[\frac{6v^2}{\lambda^4\lambda_z^2} + 2\right], \tag{27a}$$

$$g_{I_4} = 8k_1\lambda^2 e^{\bar{k}_1(I_4-1)^2}sin^4\beta + 4k_1 e^{\bar{k}_1(I_4-1)^2}sin^2\beta[I_4-1] + 16\bar{k}_1 k_1\lambda^2 e^{\bar{k}_1(I_4-1)^2}sin^4\beta[I_4-1]^2. \tag{27b}$$

For the ground substance, one can immediately notice that $g_{I_1} > 0$ for positive values of λ_z, λ and v. For the fibers, taking $k_1 > 0$ and $\bar{k}_1$, we notice that $g_{I_4} = 0$ for $\beta = 0$, i.e. when fibers are oriented in the axial direction. Further discussions regarding (27b) are given in Section 5.1.

3.3 Bending Bifurcation

Figure 4 depicts bending bifurcation of a circular cylinder. To study bending bifurcation it is not necessary to simplify the form of δu given in (19) any further. It is straight forward to show (see [11]) that the bending bifurcation (or composite mode) occurs when

$$h = \sigma_{\theta\theta} - 2\sigma_{zz} = 0. \tag{28}$$

If $h < 0$ the membrane is stable, whereas if $h > 0$ the membrane is unstable. For the material model under consideration, the bending bifurcation condition (28) can be written as

$$h = h_{I_1} + h_{I_4} = 0, \tag{29}$$

in which the term h_{I_1} is due to the mechanical behavior of the ground substance (8), and the term h_{I_4} results from the mechanical behavior of the fibers (14). It follows that

$$h_{I_1} = \frac{\mu v^{q-2/3}(\lambda^4\lambda_z^2 - 2\lambda^4\lambda_z^2 + v^2)}{(\lambda^2\lambda_z^2)}, \tag{30a}$$

$$h_{I_4} = -4k_1 e^{\bar{k}_1(I_4-1)^2}[2\lambda_z^4 cos^4\beta - 2\lambda_z^2 cos^2\beta + \lambda^2 sin^2\beta - \lambda^4 sin^4\beta + \lambda^2\lambda_z^2 cos^2\beta sin^2\beta]. \tag{30b}$$

4. Bifurcation for W_m, the Ground Substance without Fibers

Many articles on bifurcation of a cylindrical membrane have their focus on a single mode of bifurcation, whereas these modes of bifurcation may not occur as isolated events. One mode of bifurcation may join another mode during the inflation process, i.e., one mode may occur at an earlier stage of the inflation process, and another mode may then follow at a later stage of the inflation process. On the other hand, due to a change in the perfect cylindrical geometry, after the occurrence of the first bifurcation mode, a second bifurcation mode may not occur at all. In order to understand the order of occurrence and coupling of bifurcation modes, we first study the bifurcation modes in the different constituents individually before we turn to the examination of bifurcation in fibrous materials.

Let us consider a ground substance material without fibers for which the mechanical behavior of the material is solely determined by the strain energy density (8). It follows easily that

$$\widehat{W} = \widehat{W}_m = \frac{\mu\mu v^{q-2/3}}{2}\left(\frac{v^2}{\lambda^2\lambda_z^2} + \lambda^2 + \lambda_z^2 - 3v^{2/3}\right). \tag{31}$$
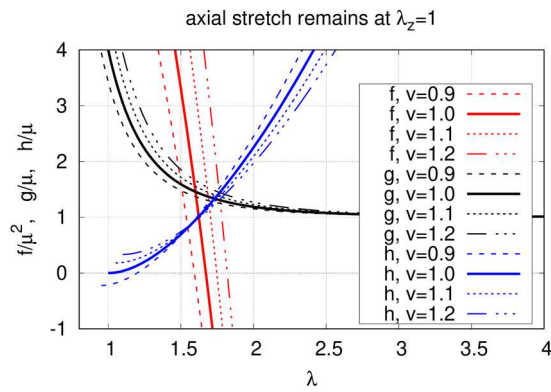
Fig. 5. Values (normalized) of $f = f_{I_1}$, $g = g_{I_1}$ and $h = h_{I_1}$ vs λ for $\lambda_z = 1$ and a ground substance material (without fibers) with different values of the swelling parameter v. Red curves give values of the bulging function $f = f_{I_1}$, black curves give values of the prismatic function $g = g_{I_1}$ and blue curves give values of the bending function $h = h_{I_1}$. Negative values of f and g and positive values of h are associated with bulging bifurcation, prismatic bifurcation and bending bifurcation, respectively, i.e. with unstable configurations of the initially perfect circular cylindrical membrane. The undeformed and unswollen configuration of the membrane is given by the point $(\lambda, \lambda_z) = (1,1)$. Close to this configuration for $v = 1$ as well as greater than 1 (swelling) and $\lambda > 1$ (inflation of the membrane), values of h are positive, which means that bending is expected as soon as the membrane begins to be inflated. In addition, it is clear that the values of λ obeying $f = 0$ are also associated with values $h>0$. This is an indication that while bulging does not give the onset of bifurcation (it is not the lower bound for bifurcation), during postbifurcation (after bending occurs) bulging might be expected. Values of g are positive; therefore, prismatic bifurcation is not expected. Nevertheless, prismatic bifurcation cannot be ruled out completely during post-bifurcation since, among other reasons, the g-based analysis only characterizes the first prismatic bifurcation mode.

Moreover, the pressure inflation relation (16) takes the form

$$P = \frac{H}{R} \frac{\mu v^{q-2/3}}{\lambda^4 \lambda_z^3} [\lambda^4 \lambda_z^2 - v^2]. \tag{32}$$

To prevent negative values of (inflation) pressure P it follows from (32) that $\lambda^4 \lambda_z^2 \geq v^2$. For a ground substance without fibers, the bifurcation conditions (22), (26), and (29) reduce to $f = f_{I_1} = 0$, for bulging bifurcation, $g = g_{I_1} = 0$ for prismatic bifurcation, and $h = h_{I_1} = 0$ for bending bifurcation. It is clear that these conditions are independent of the swelling-dependent shear modulus $\mu v^{q-2/3}$. Indeed, this is true for the ground substance without fibers, while bifurcation of a ground substance with embedded fibers is affected by swelling-dependence ground substance stiffness. This will be shown in Section 6. Nevertheless, for illustrative purposes, we turn our attention to swelling-independent ground substance stiffness for which $q = 2/3$. This case is representative of other situations. We also establish the role of the axial stretch.

4.1 Swelling-independent ground substance stiffness and a fixed axial stretch

For $q = 2/3$, the shear modulus of the strain energy density of the ground substance (8) is independent of swelling. Under this circumstance and $\lambda_z \geq 1$, Fig. 5 shows values of $f = f_{I_1}$, $g = g_{I_1}$ and $h = h_{I_1}$ vs λ for different values of the swelling parameter v. Let us focus on the bifurcation modes separately. Bifurcation is associated with either $f = 0$, $g = 0$ or $h = 0$. The undeformed and unswollen configuration of the membrane is given by the point $(\lambda, \lambda_z) = (1,1)$. Values of λ obeying $f = 0$ (red curves) for bulging are greater for greater values of swelling. Blue curves for bending bifurcation show that a swollen (v > 1) and an unswollen ($v = 1$) material is unstable as inflation begins, i.e., $h > 0$ close to $(\lambda, \lambda_z) = (1,1)$. On the other hand, deswelling ($0 < v < 1$) can stabilize the material with respect to the bifurcation modes under consideration for values close to $(\lambda, \lambda_z) = (1,1)$ since $h < 0$. For a given value of v, the values of λ obeying $f = f_{I_1} = 0$, are associated with $h = h_{I_1} > 0$, i.e., comparing corresponding curves of f and h, it is easy to conclude that bending occurs at smaller values of λ (earlier stages of inflation) and it is the lower bound for bifurcation.

Black curves for prismatic bifurcation are associated with values $g = g_{I_1} > 0$ for the herein considered parameter values. Indeed, from (27a) one can immediately notice that $g_{I_1} > 0$ for positive, and therefore physically meaningful, values of λ_z, λ, and v. This result is in agreement with results given in [36].

4.2 Unswollen ground substance and different axial stretches

In this section, we compare the different bifurcation modes for an unswollen material ($v = 1$) subject to several values of the axial stretch λ_z. We follow accordingly the procedure, arguments, and results established in Sec 4.1.1. For $q = 2/3$ and $v = 1$, Fig. 6 shows values of $f = f_{I_1}$, $g = g_{I_1}$ and h= h_{I_1} vs λ for different values of the axial stretch λ_z. Values of λ obeying $f = 0$, (red curves) for bulging are smaller for greater values of the axial stretch. Blue curves for bending bifurcation show that an extended membrane $(\lambda_z > 1,)$ is stable as inflation begins, i.e., $h < 0$, close to $(\lambda, \lambda_z) = (1,1)$. In Fig. 6 , for a given λ_z, it is not always easy to deduce the lower bound for bifurcation since it is not easy to check the value of $h = h_{I_1}$ for the value of λ obeying $f = f_{I_1} = 0$. Clearly, for $\lambda_z = 1$ the lower bound is bending while for $\lambda_z = 1.3$ the lower bound is bulging. While values $f = 0$, red curves, shift to smaller values of the azimuthal stretch λ for greater values of the axial stretch λ_z, the opposite effect is observed for bending bifurcation, i.e., blue curves shift downwards and to the right side (values $h < 0$) for greater values of λ_z. Nevertheless, one can conclude that the extension of the membrane stabilizes the material against bending bifurcation.

The observations from Fig. 6 immediately leads us to establish the deformation conditions associated with the lower bifurcation mode, which can be either bulging or bending. This is obtained by establishing points (λ, λ_z) that simultaneously obey $f_{I_1} = 0$ and $h_{I_1} = 0$ for a given material. Figure 7 shows points (λ, λ_z) obeying $f_{I_1} = 0$ (red curve) and $h_{I_1} = 0$ (blue curve) for an unswollen material $v = 1$. When $(\lambda, \lambda_z) = (\lambda_{fh}, \lambda_{z,fh}) = (1.57, 1.18)$ both curves intersect and bulging and bending bifurcation are initiated simultaneously. It follows that for $\lambda_z < 1.18$ the lower bifurcation mode is bending while for $\lambda_z > 1.18$ the onset of bifurcation is given by bulging.
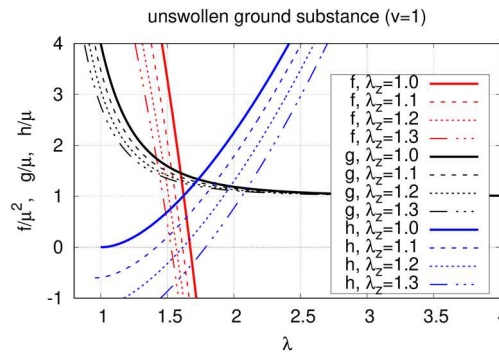
Fig. 6. Values (normalized) of $f = f_{I_1} = 0$, $g = g_{I_1} = 0$ and $h = h_{I_1} = 0$ vs λ for an unswollen ground substance material $(v = 1)$ without any fibers and different values of the axial stretch λ_z. Negative values of f and g and positive values of h are associated with bulging bifurcation, prismatic bifurcation, and bending bifurcation, respectively. For $\lambda_z = 1$ and the associated value of λ obeying $f = f_{I_1} = 0$, it is clear that $h = h_{I_1} > 0$ and, whence, bending is the lower bifurcation mode. On the other hand, for $\lambda_z = 1.3$ and the associated value of λ obeying $f = f_{I_1} = 0$, it is clear that $h = h_{I_1} < 0$ and it follows that bulging is the lower bifurcation.
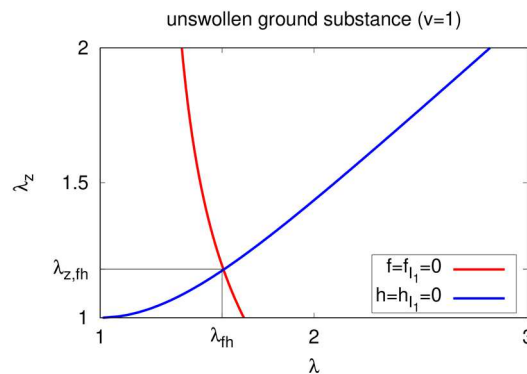

Fig. 7. Points (λ, λ_z) obeying $f = f_{I_1} = 0$ (red curve) and $h = h_{I_1} = 0$ (blue curve) for a ground substance without fibers that remains unswollen v = 1. Both curves intersect for $(\lambda, \lambda_z) = (\lambda_{fh}, \lambda_{z,fh}) = (1.57,1.18)$ so that bulging and bending bifurcation are initiated simultaneously. It follows that for $\lambda_z > 1.18$ the onset of bifurcation is given by bulging while for $\lambda_z < 1.18$ the lower bifurcation mode is bending.

5. Bifurcation for W_f, the Fibers

In this section, we assume that the mechanical behavior given by the ground substance material is negligible compared to the mechanical behavior given by the fibers. One could think that this is a highly anisotropic material. The mechanical properties of the fibers dominate the properties of the matrix, i.e. $\mu/k_1 \to 0$. This is a useful case to understand the role of the fibers in the bifurcation of cylinders although it is a subtle case with limitations since the matrix response cannot be completely disregarded for a well-posed constitutive equation. Nevertheless, the purpose of this analysis is to illustrate the fibers' effect with regard to bifurcation and this is described in what follows.

The strain energy density function W for this material is completely determined via (14),

$$\widehat{W} = \widehat{W}_f = \frac{k_1}{\bar{k}_1}\left[e^{\bar{k}_1\left(\lambda_z^2 cos^2\beta + \lambda^2 sin^2\beta - 1\right)^2} - 1\right]. \tag{33}$$

The pressure-inflation relation (16) for the fibers takes the form

$$P = 4\frac{k_1}{\lambda_z}\frac{H}{R}e^{\bar{k}_1\left(\lambda_z^2 cos^2\beta + \lambda^2 sin^2\beta - 1\right)^2}sin^2\beta\left[\lambda_z^2 cos^2\beta + \lambda^2 sin^2\beta - 1\right], \tag{34}$$

which is equal to zero for $\beta = 0$ or for $\lambda_z^2 cos^2\beta + \lambda^2 sin^2\beta = I_4 = 1$. Furthermore, the bifurcation conditions given in (22), (26), and (29) reduce to $f = f_{I_4} = 0$ for bulging bifurcation, $g = g_{I_4} = 0$ for prismatic bifurcation, and $f = f_{I_4} = 0$ for bending bifurcation. It is clear that these conditions are independent of k_1.

We recall that in the limit

$$\lim_{\bar{k}_1 \to 0}\frac{k_1}{\bar{k}_1}\left[e^{\bar{k}_1\left(\lambda_z^2 cos^2\beta + \lambda^2 sin^2\beta - 1\right)^2} - 1\right] = k_1[\lambda_z^2 cos^2\beta + \lambda^2 sin^2\beta - 1]^2, \tag{35}$$

i.e. the strain energy density for the fibers (33) approaches the so-called standard reinforcing model [40, 50–52]. Note that this standard form, the right hand side of (35), is not only the limiting case for the exponential form since it (the standard form) can be derived from logarithmic forms of strain energy densities for fibers, see, for instance [53]. In what follows we analyze separately two cases: one obeying that $\bar{k}_1 \to 0$ for which the strain energy is the so-called standard reinforcing model, and the exponential, which is used for any other value of k_1. In the modeling of collagen fibers in arterial wall tissue, fibers are often taken to be incapable of supporting compression [46]. For that reason, fibers are considered to contribute if and only if $I_4 \geq 1$.

5.1 The standard reinforcing model

We first consider the specification $\bar{k}_1 \to 0$, for which the strain energy density (33) yields the so called standard reinforcing model (35). Figure 8 shows values (normalized) of $f = f_{I_4}$ (red curves), $g = g_{I_4}$ (black curves) and $h = h_{I_4}$ (blue curves) vs λ for different values of the axial stretch λ_z and selected values of the fiber winding angle β. More in particular, Figure 7 (a) is for $\beta = $

$\pi/6$, Figure 7 (c) is for $\beta = \pi/3$ and Figure 7 (e) is for $\beta = \pi/2$, while Figure 7 (b) is just a magnification of Figure 7 (a) near the point (1,0) and, similarly, Figure 7 (d) is just a magnification of Figure 7 (c) near the point (1,0). The labeled curve styles shown in Figure 7 (a) apply to the other panels. In Fig. 8 (e), for $\beta = \pi/2$, there is only one curve for $f = f_{I_4}$ as well as for $g = g_{I_4}$ and $h = h_{I_4}$, since the fibers are in the azimuthal direction and $f = f_{I_4}$, $g = g_{I_4}$ and $h = h_{I_4}$ are independent of λ_z. One can immediately notice that prismatic bifurcation is not expected to occur since $g > 0$.

Let us pay attention to the curves for $\lambda_z = 1.2$, in Figure 8 (b) ($\beta = \pi/6$) and Figure 8 (d) ($\beta = \pi/3$). The curves show that around the undeformed configuration $(\lambda, \lambda_z) = (1,1)$ there are points (λ, λ_z) obeying that $h < 0$ (blue curves) while for these points f (red curves) is always positive. Furthermore, for $\lambda > 1$ blue curves change from negative to positive values while for these points the values of f (red curve) are positive. This means that the lower bifurcation mode is bending. This argument also applies to the other values of λ_z. It is also shown in 8 (a) and Figure 8 (c), that the f-curves have a maximum, which, comparing panels (a) and (c), decreases for greater values of β. In addition, Figure 7 (e) shows that f is negative while h is positive, which, in turn, means that as $\beta \to \pi/2$ bending and bulging may occur almost simultaneously. It follows that, as the membrane is inflated, greater values of β make the membrane more unstable with regard to both bulging and bending. Conversely, smaller values of β make the membrane more stable with regard to bulging and bending. It also follows for a given β that greater values of λ_z stabilize the membrane with respect to bending since the values of λ associated with $h = 0$ are greater as λ_z increases (see, for instance, panel (b)).
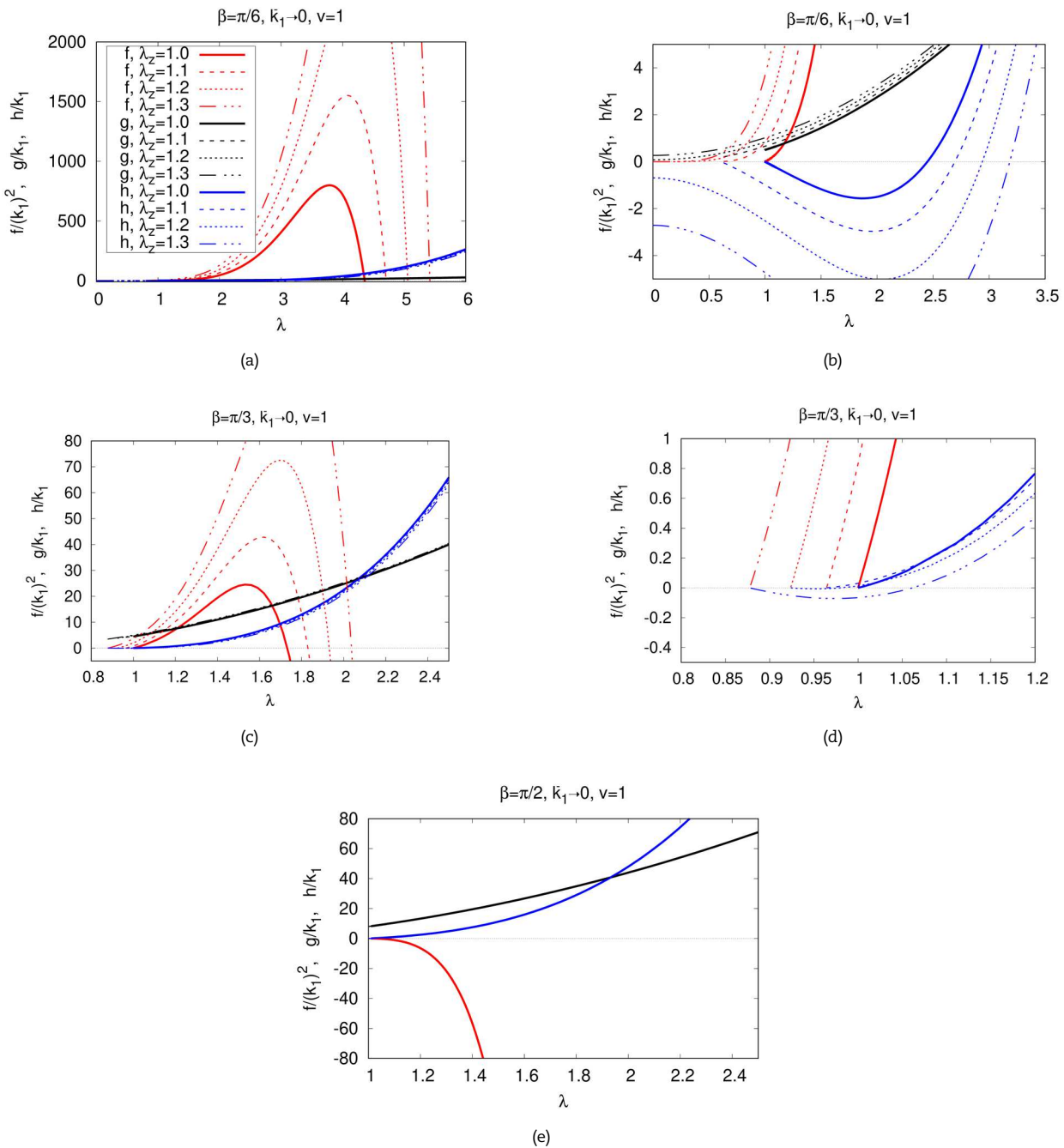
Fig. 8. Values (normalized) of $f = f_{I_4}$ (red curves), $g = g_{I_4}$ (black curves) and $h = h_{I_4}$ (blue curves) vs λ for different values of the axial stretch λ_z and selected values of the fiber winding angle β. The legend in panel (a) applies to all panels. More in particular, panel (a) is for $\beta = \pi/6$, while its magnification is given in panel (b); panel (c) is for $\beta = \pi/3$, while its magnification is given in panel (d); and panel (e) is for $\beta = \pi/2$. In the latter case, since the fibers are perpendicular to the axial direction, the results are independent of the axial stretch λ_z., so that there are only three curves, one for $f = f_{I_4}$ as well as one for $g = g_{I_4}$ and $h = h_{I_4}$.

The different panels of Fig. 8 show results for selected values of the fiber winding angle β. With the purpose of gaining a complete illustration of the analysis, now we broaden our attention and focus on the development of bifurcation conditions for all possible values of β. Results are shown in Fig. 9 for different values of the axial stretch λ_z. Since $g > 0$ we just focus on f and h.

Figure 9 shows (normalized) values of $f = f_{I_4}$ (red curves) and $h = h_{I_4}$ (blue curves) as a polar plot with respect to the angle β for different values of the axial stretch λ_z and $\lambda = 1.5$, panel (a) and its magnification, panel (b), and $\lambda = 2$, panel (c) and its magnification, panel (d). The symmetry of the results is due to the fact that both fiber families are mechanically equivalent and are symmetrically disposed with respect to the axial direction. It follows that it is sufficient to consider values $\pi/2 \geq \beta \geq 0$. More in particular, Figure 9 shows that close to and around $\beta = 0$, $f = f_{I_4} > 0$ (red curves) and $h = h_{I_4} < 0$ (blue curves), i.e., there is neither bulging nor bending. On the other hand, Figure 9 shows that close to and around $\beta = \pi/2$, $f = f_{I_4} < 0$ (red curves) and $h = h_{I_4} > 0$ (blue curves), i.e., the membrane is unstable with respect to both bulging and bending. Panel (b) for $\lambda = 1.5$ shows that $f = f_{I_4} = 0$ for values of β a little greater than $\pi/3$, while Panel (d) for $\lambda = 2$ shows that $f = f_{I_4} = 0$ for values of β a little smaller than $\pi/3$, i.e. greater values of λ require smaller values of β for the membrane to be stable regarding bulging. This means that smaller values of β stabilize the membrane with respect to bulging. A similar argument follows for the blue curves associated with bending bifurcation although numbers are not given. The values (and interpretation) of these plots are in agreement with the ones given in Figure 8.

This analysis has disentangled deformed configurations given by points (λ, λ_z), around the undeformed configuration $(\lambda, \lambda_z) = (1,1)$, that have been understood in terms of bending and bulging. This limiting case of just fibers has shown the effect of the fibers for different values of β although this case is just an extreme idealization. To interpret the results further and understand the limitations and the subtle scenario of this fiber-only case let us consider that the tube has been subjected first to a given uniaxial tension so that $\lambda = 1/\sqrt{\lambda_z}$. The value of λ_z is then fixed and the tube inflated, with λ increasing. This path of deformation is acceptable if and only if $I_4 \geq 1$, which also depends on β. Indeed, for $\beta = \pi/6$ it is easy to show that this path of deformation is admissible for any value of λ_z. For greater values of β, for instance $\beta = \pi/3$, and some values of λ_z, the value of λ given by $\lambda = 1/\sqrt{\lambda_z}$ is associated, in turn, with $I_4 < 1$, which is not permitted. Our analysis, then, considers for the λ_z at hand a greater value of λ until $I_4 = 1$, which is associated with the value $P = 0$. To eliminate completely the matrix response and simultaneously consider that $I_4 \geq 1$ leaves that scenario, which only considers some deformations. This fiber kinematics behavior also applies to the next section and will be exploited later on to study and understand bifurcation for a matrix reinforced with fibers.

5.2 The exponential form

We now turn to study the bifurcation conditions for the exponential form (33), i.e., for values of $\bar{k}_1$ that are greater than zero. From (27b), it is easy to show that $g = g_{I_4} > 0$, and we do not focus on prismatic bifurcations. Figure 10 illustrates the effect of $\bar{k}_1$ on both bulging and bending bifurcation. In particular, curves in Figure 10(a), $\beta = \pi/6$, and Fig. 10 (b), $\beta = \pi/3$, give, for different values of the axial stretch λ_z, points $(\lambda, \bar{k}_1)$ that obey $f = f_{I_4} = 0$ (bulging, red curves) and points $(\lambda, \bar{k}_1)$ that obey $h = h_{I_4} = 0$ (bending, blue curves).

Blue curves are vertical lines. The reason is the following. The bending bifurcation condition (30b) for $h = h_{I_4} = 0$ becomes

$$h_{I_4} = 2\lambda_z^4 \cos^4\beta - 2\lambda_z^2 \cos^2\beta + \lambda^2 \sin^2\beta - \lambda^4 \sin^4\beta + \lambda^2 \lambda_z^2 \cos^2\beta \sin^2\beta = 0, \qquad (36)$$

which depends on the stretches λ and λ_z as well as the angle β, but it is independent of the parameter $\bar{k}_1$. Furthermore, it follows from (30b) that h is negative for $\beta = 0$ while it is positive for $\beta = \pi/2$ under fiber extension ($\lambda > 1$). Hence, smaller values of β stabilize the membrane with respect to bending in agreement with the result established for the standard reinforcing model.
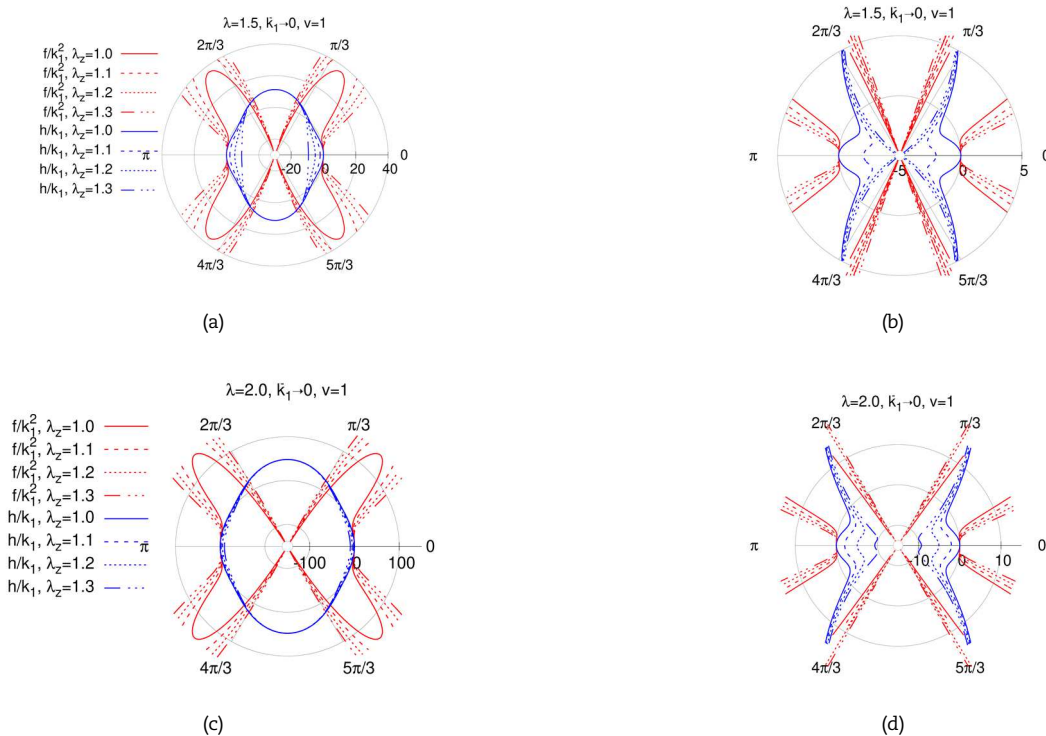

(a)

(b)

(c)

(d)

Fig. 9. Values of $f = f_{I_4}$ (red curves) and $h = h_{I_4}$ (blue curves) as a polar plot with respect to the angle β for different values of λ_z and $\lambda = 1.5$, panel (a) and its magnification panel (b), and $\lambda = 2$, panel (c) is its magnification panel (d). Left panels (a) and (c) show the general development of f/k_1^2 and h/k_1, whereas right panels (b) and (d) highlight the behavior of these functions close to their zero values. The symmetry of the results is due to the fact that both fiber families are mechanically equivalent and are symmetrically disposed with respect to the axial direction.
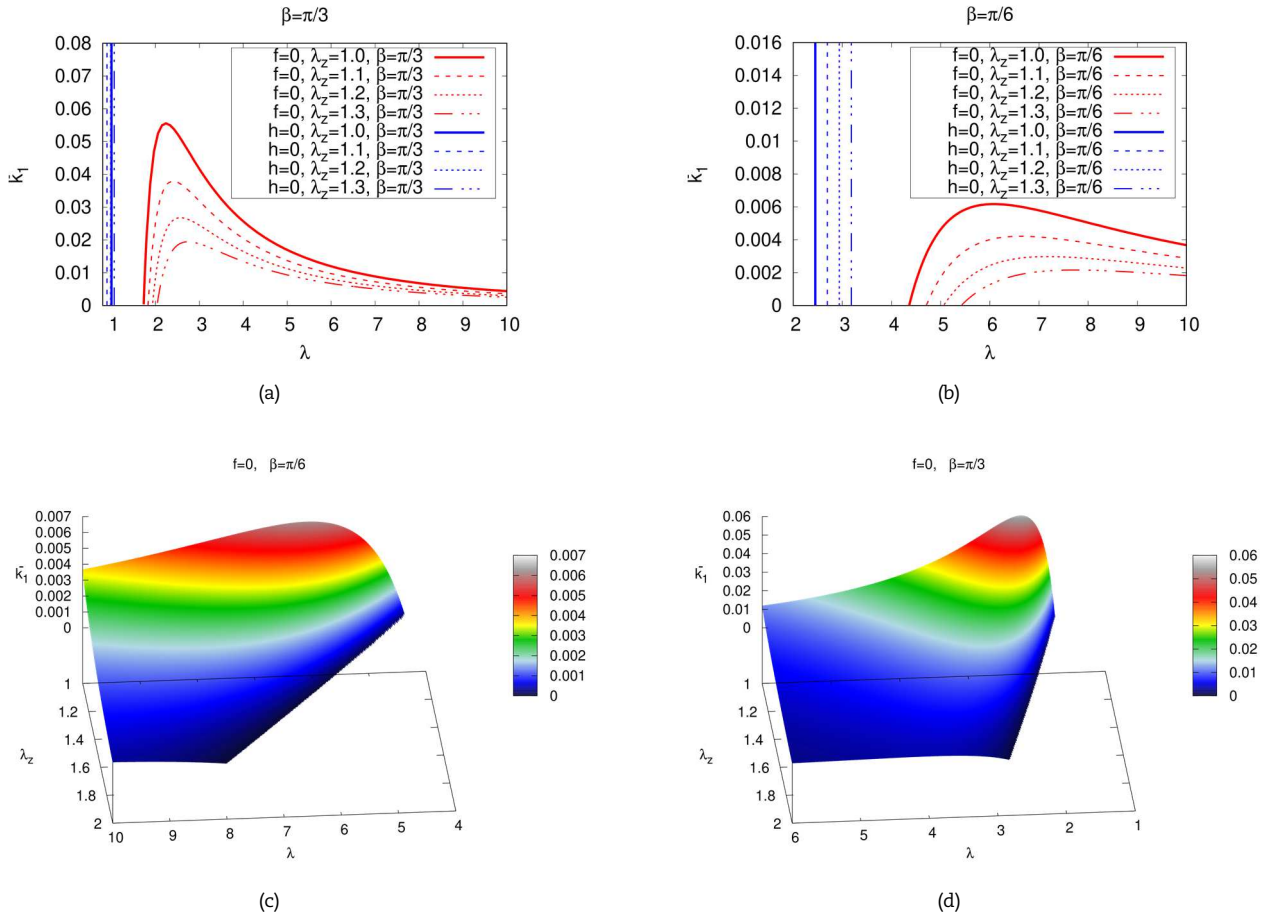
(a)

(b)

(c)

(d)

Fig. 10. For different values of λ_z, the top panels (a), for $\beta = \pi/6$, and (b), for $\beta = \pi/3$, show values of $\bar{k}_1$ vs λ obeying either $f = 0$ (bulging bifurcation, red curves) or $h = 0$ (bending bifurcation, blue curves). The bottom panels (c) and (d) give the corresponding values of λ, λ_z,, and $\bar{k}_1$ that fulfill $f = 0$ given in panels (a) and (b), respectively.
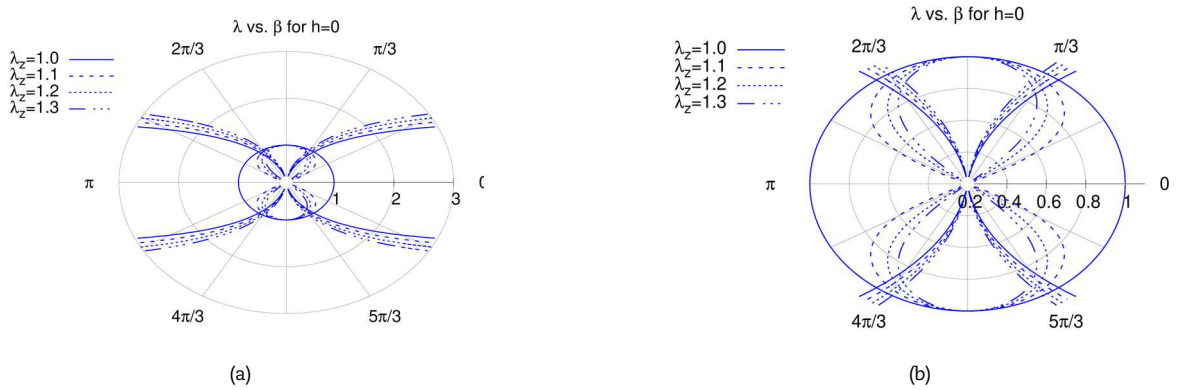

(a)

(b)

Fig. 11. Curves give values of circumferential stretch λ (radial value in the plot) and the fiber winding angle β obeying $h = 0$ for different values of the axial stretch λ_z. Panel (b) is a magnification of panel (a). In panel (a), it is easy to deduce that when $h = 0$ for $\beta = \pi/6$ greater values of λ are associated with greater values of λ_z, in agreement with the order shown by the blue curves in Fig. 10 (a). Similarly, in panel (b), it is easy to deduce that when $h = 0$ for $\beta = \pi/3$ greater values of λ are not associated with greater values of λ_z, in agreement with the values of λ given by the blue curves shown in Fig. 10 (b).

The top panels (a) and (b) of Fig. 10 show that for sufficiently large values of $\bar{k}_1$ the condition $f = f_{I_4} = 0$ is not satisfied, while for sufficiently small values of $\bar{k}_1$ the condition $f = f_{I_4} = 0$ is satisfied by just one point $(\lambda, \bar{k}_1)$. On the other hand for a given value of $\bar{k}_1$ in between these two cases, $f = f_{I_4} = 0$ is satisfied by two values of λ. As the membrane is inflated panels (a) and (b) show that the lower bifurcation mode is bending. Furthermore, during post-bifurcation, it may be followed by bulging bifurcation for sufficiently small values of $\bar{k}_1$. This might be expected although it is not certain since the membrane is not a perfect circular cylinder. Nevertheless, for sufficiently large values of $\bar{k}_1$ bulging is not expected even after bending. Furthermore, a simple comparison of the curves $f = f_{I_4} = 0$ in panels (a) and (b) establishes that smaller values of β stabilize the membrane with respect to bulging in agreement with the result established for the standard reinforcing model. In addition, an interesting observation for $h = h_{I_4} = 0$ (blue curves) by comparison of Fig. 10 (a) and (b) is the shift in the order of these curves for the different values of the axial stretch λ_z due to the change of the value of β. In Fig. 10 (a) the blue curves are ordered accordingly with the greater values of λ_z, i.e. greater values of λ are associated with greater values of λ_z, which does not occur in Fig. 10 (b). This motivates the analysis of $h = 0$ with the winding angle.
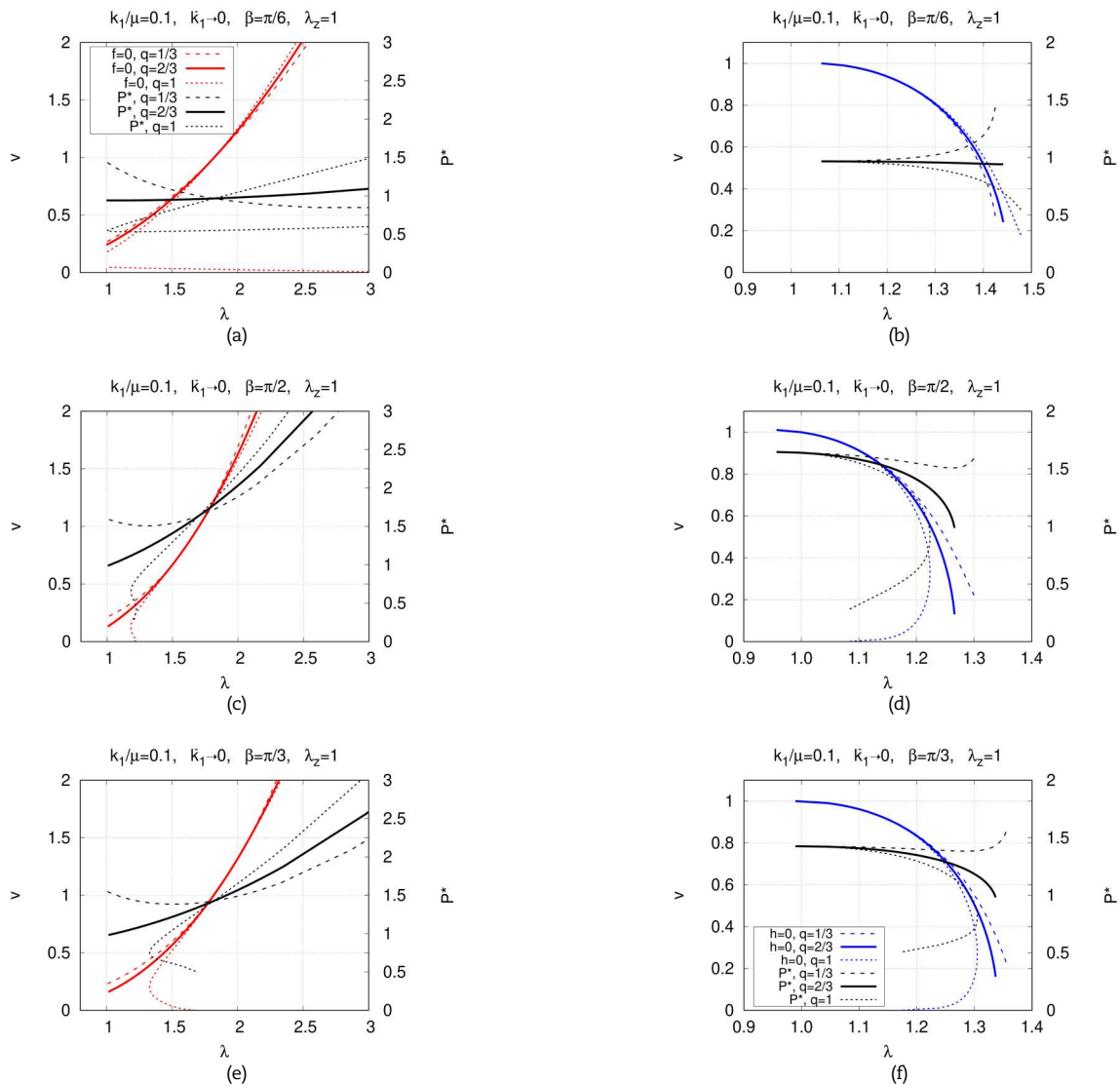
Fig. 12. Values of v vs λ obeying either f = 0 (red curves in panels (a), (c) and (e)) or h = 0 (blue curves in panels (b), (d) and (f)) as well as their associated values of $P^* = PR/(\mu H)$ vs λ (black curves) for $\lambda_z = 1.0$, three selected values of q ($q = 1/3$, $q = 2/3$, and $q = 1$) and some values of β, in particular, $\beta = \pi/6$ (panels (a), (b)), $\beta = \pi/3$ (panels (c), (d)) and $\beta = \pi/2$ (panels (e), (f)). Results show for $v > 0.5$ that q does not have a qualitative effect on the bifurcation curves but it does have a qualitative effect on pressure curves.

The blue curves in Figure 11 give values of the circumferential stretch λ (radial value) and the fiber winding angle β that obey the bending bifurcation condition $h = h_{I_4} = 0$ for different values of the axial stretch λ_z. Figure 11 (b) is a magnification of Fig. 11 (a). Results for $\lambda = 1$ are associated with the trivial solution for an unloaded (undeformed) tube. The values of λ given by the blue curves in Fig. 10 (a) can be deduced from Figure 11 (a) when $\beta = \pi/6$. Similarly, the values of λ given by the blue curves in Fig. 10 (b) can be deduced from Figure 11 (b) when $\beta = \pi/3$.

6. Bifurcation for the Ground Substance Matrix with Fibers

Previous sections deal with bifurcation for the ground substance and for the fibers separately. In this section we turn to consider a ground substance with embedded fibers to examine bifurcation phenomena that occur when both constituents define the elastic behavior of the cylinder. We consider deformations for which the inflation pressure is held by both the fibers and the matrix, i.e. the fibers are extended since otherwise the analysis involves just the matrix (which was given previously in Section 4.1) and simultaneously the matrix also supports pressure. The following results are restricted to bulging and bending since prismatic bifurcations have been shown not to play a major role.

For the material at hand, the parameter q describes the change in the ground substance stiffness with swelling v, and, therefore, it is associated with the ratio of the ground substance stiffness to the fiber stiffness. For swelling, $v > 1$, greater values of $v^{q-2/3}$ are associated with $q > 2/3$ (the ground substance behavior becomes relevant compared with the one given by fibers) while smaller values of $v^{q-2/3}$ are associated with $q < 2/3$ (the ground substance behavior is less relevant than the one associated with the fibers). Conversely, for deswelling, $v < 1$, greater values of $v^{q-2/3}$ are associated with $q < 2/3$ while smaller values of $v^{q-2/3}$ are associated with $q > 2/3$. The effect of this stiffness change on the occurrence of bifurcation is illustrated with the next analysis in which the strain energy density function W in (7) is composed of both a ground substance with an elastic behavior W_m given by (8) and embedded fibers with the strain energy density function W_f given by (14). For the elastic parameters we take $k_1/\mu = 0.1$ and $\bar{k}_1 \to 0$ (standard reinforcing model). Values of the dimensionless (and normalized) pressure $P^* = PR/(\mu H)$ are also shown.
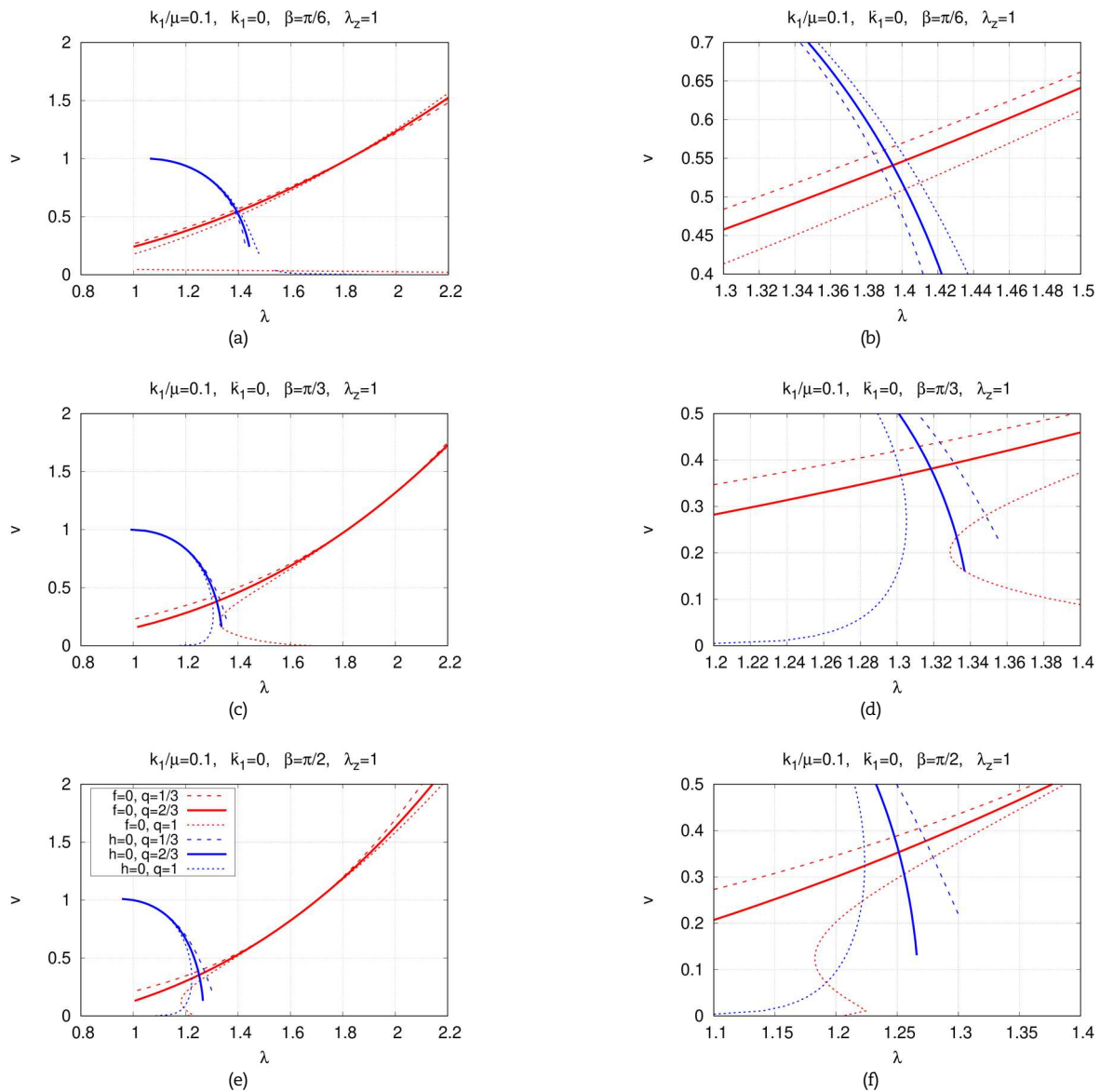
Fig. 13. This figure gives simultaneously the bulging and bending bifurcation curves shown in Fig. 12 and, therefore, establishes accordingly the expected onset of bifurcation for $\lambda_z = 1.0$. Panels (b), (d) and (f) are magnifications of panels (a), (c) and (e), respectively, near the region in which these curves intersect each other.

6.1 Bulging and bending

Figure 12 shows values of v vs λ obeying either $f = 0$ (red curves in panels (a), (c) and (e)) or $h = 0$ (blue curves in panels (b), (d) and (f)) as well as their associated values of P^* vs λ (black curves) for $\lambda_z = 1$, three selected values of q ($q = 1/3$, $q = 2/3$, and $q = 1$) and some values of β, in particular, $\beta = \pi/6$ (panels (a), (b)), $\beta = \pi/3$ (panels (c), (d)) and $\beta = \pi/2$ (panels (e), (f)). Values of $v < 0.5$ are shown for completeness although these are extreme cases and in what follows we focus on values $v > 0.5$. In general, for $v > 0.5$, the bulging bifurcation curves ($f = 0$) are monotonically increasing. On the other hand, the bending bifurcation curves ($h = 0$) are monotonically decreasing. The parameter q shows a quantitative effect rather than a qualitative one on the bifurcation curves since they keep close to each other in all panels. On the other hand, the associated pressure curves show a qualitative effect due to q and, in particular, they are not monotonically increasing or decreasing. A variety of results depending on v, β and λ are shown in the different panels. Nevertheless, panels (c) and (e) in Fig. 12 (for sufficiently large values of β) show that for sufficiently large values of λ (around $\lambda = 1.7$) pressure curves are monotonically increasing and these values are associated with both $v > 1$ and $v < 1$. With regard to bending, for sufficiently large values of v, i.e., $v > 0.8$, pressure curves are monotonically decreasing.

We now turn our attention to establish the lower bound for bifurcation in an extended and pressurized cylinder membrane capable of swelling. Figure 13 gives simultaneously the bulging and bending bifurcation curves shown in Fig. 12 and, therefore, establishes accordingly the expected onset of bifurcation for $\lambda_z = 1$. The panels (b), (d) and (f) are magnifications of panels (a), (c) and (e), respectively, near the region in which these curves intersect each other. In general bulging gives the onset of bifurcation under two situations: 1) for sufficiently large values of swelling $v > 1$ as well as 2) for sufficiently large values of deswelling $v < 1$, and in both cases the value of v depends on the axial stretch. During post-bifurcation bulging might be coupled with bending, which occurs in an abdominal aortic aneurysm (AAA).

Our analysis has considered that both matrix and fibers hold pressure. This means that fibers are extended. To interpret further the analysis and the results let us turn our attention to the effect that fiber extension has on pressure vs λ curves, which is the subject of the next section.
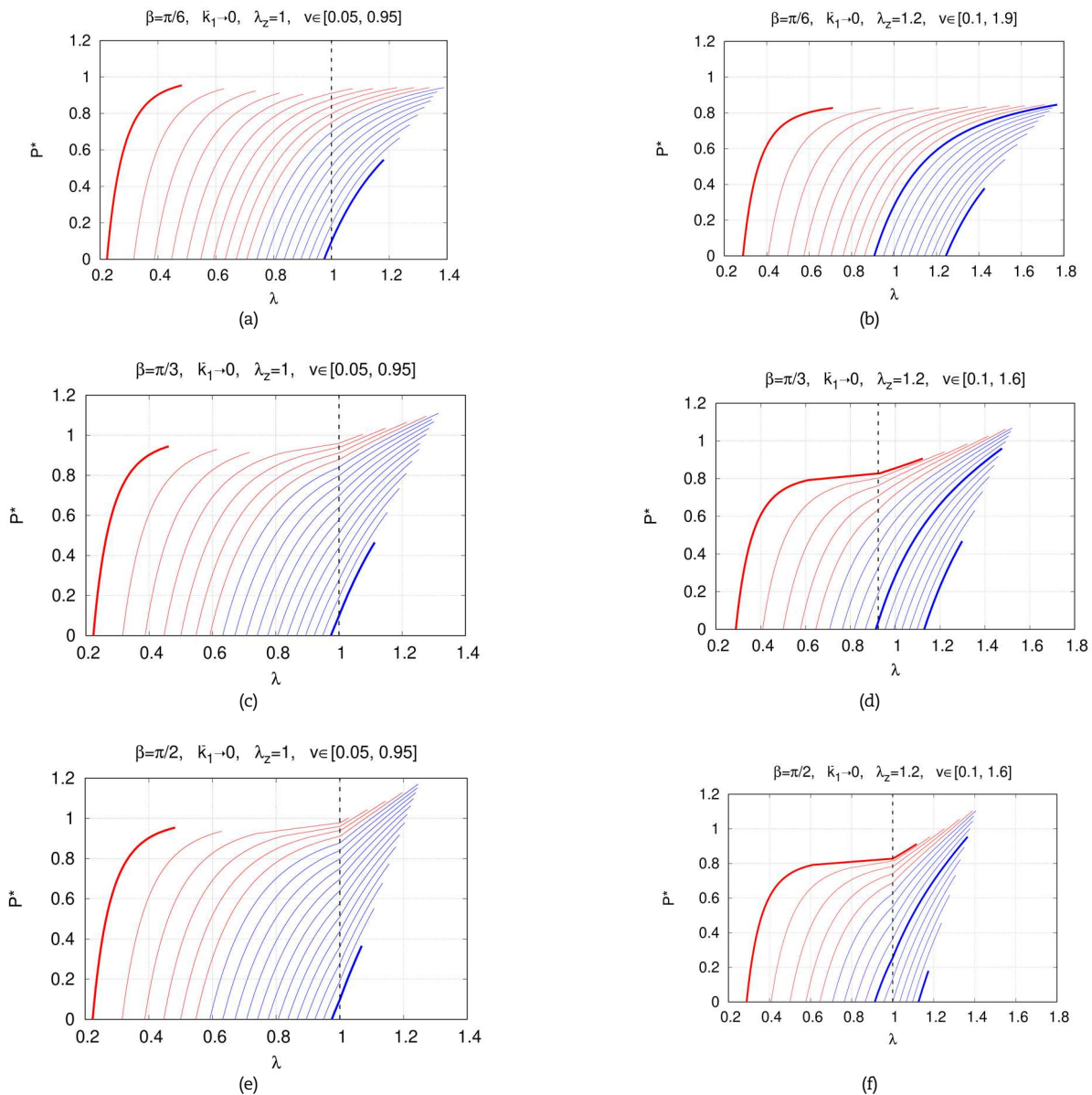
Fig. 14. Values of pressure P^* vs λ that are stable with regard to both bulging and bending, taking $q = 2/3$, $k_1/\mu = 0.1$ and $\bar{k}_1 \to 0$. Top panels (a), (b) are for $\beta = \pi/6$; middle panels (c), (d) are for $\beta = \pi/3$; and bottom panels (e), (f) are for $\beta = \pi/2$. For the red curves the stable inflation process is interrupted by bulging, whereas for the blue curves the stable inflation is interrupted by bending bifurcation.

6.2 Ground substance with embedded fibers that may or may not be extended

The previous examples analyze bifurcation modes in a cylinder, in which both the ground substance and the fibers contribute to the elastic behavior. These examples examine deformations (combinations of azimuthal and axial stretches), as well as values of the swelling field and the parameter q associated with bulging or bending. A cylinder may inflate or deflate due to a change in the pressure or due to swelling. Similarly, as a result of remodeling processes, the stiffness of the fibers and their orientation may change. As a result, fibers may or may not be extended and here we analyze this effect in the context of our previous results. From (11a) one can conclude that $I_4 = 1$ if

$$\lambda = \lambda_0 = \sqrt{\frac{1 - \lambda_z^2 cos^2\beta}{sin^2\beta}}. \tag{37}$$

Consider a tube which is subjected to an inner pressure P for a given axial stretch λ_z, a value of v, $q = 2/3$ (matrix stiffness is independent of swelling), a value of β, $k_1/\mu = 0.1$ and $\bar{k}_1 \to 0$ (standard reinforcing model). Let us analyze the relation between the inflation pressure and the deformation λ given by (16). We consider also deformations for which the fibers do not contribute since they are not extended and just the matrix holds pressure. Under these circumstances, Figure 14 shows values of the normalized pressure P^* vs λ that are stable with regard to both bulging and bending bifurcation, i.e., $f > 0$ and $h < 0$, for different values of the parameters β, λ_z and v. In particular, in all panels each curve is associated with a value of v. The curve at the left of each panel is associated with the smallest value of v (indicated at the top of each panel), and greater values of v are associated with the other curves to the right. More in particular, left panels (a), (c) and (e) are for $\beta = \pi/6, \pi/3$ and $\pi/2$, respectively, $\lambda_z = 1$ and swelling values between $v = 0.05$ (left bold curve) and $v = 0.95$ (right bold curve) with increments of $\Delta v = 0.05$. Similarly, right panels (b), (d) and (f) are for $\beta = \pi/6, \pi/3$ and $/2$, respectively, $\lambda_z = 1.2$ and swelling values between $v = 0.1$ (left bold curves) and $v = 1.60$ or $v = 1.90$ (right bold curves) with increments of $\Delta v = 0.1$. The value of λ_0 for each panel is obtained easily using (37). It follows that in panel (b) fibers are extended for all values of λ. On the other hand, in the other panels a vertical dashed line indicates the value of λ_0. If $\lambda < \lambda_0$ (left of the dashed line) then the fibers are wavy or crimped and loads are only held by the matrix. If $\lambda > \lambda_0$,

then the fibers are recruited and both matrix and fibers bear loads. In the left panels, $\lambda_0 = 1$ and it is independent of the fiber winding angle β. In panel (d) $\lambda_0 = 0.923760431$ and in panel (f) $\lambda_0 = 1$.

In general, for sufficiently small values of λ_z and sufficiently large values of β (for instance, in panels (c) to (f)) if the material is deswollen and the inflation pressure is relatively small, then, the crimped or wavy fibers are not extended since this is associated with small values of λ. If the inflation pressure and swelling are sufficiently large, then, fibers resist the inflation pressure. For $\lambda > \lambda_0$ fibers are extended and curves in the panels show a change in their slopes.

7. Discussion and Outlook

This article has shown that the occurrence and the order of the bifurcation modes in a symmetrically reinforced swellable membrane tube depend on different factors, including the geometry of the examined problem, the elastic properties of the constituents, and the arrangement of the fibers. An understanding of the circumstances under which geometrical instabilities occur may help to understand the formation and propagation of aneurysms, i.e. it may help to predict such formation and its rupture.

For the swellable neo-Hookean type ground substance and for the exponential form of the fibers strain energy density function prismatic bifurcation is not expected and attention has been paid to bulging and bending. Nevertheless, it should be pointed out that our considerations for bifurcation have been restricted to fibers that cannot support compression and also to internal inflation. If, for example, an external pressure exceeds the inner pressure in the cylinder, then, the onset of instability might be given by the prismatic bifurcation (see, e.g. [36]).

It has been shown that swelling may stabilize the material [31, 34] with respect to bulging bifurcation, whereas deswelling stabilizes the material with respect to bending bifurcation. Both deswelling and axial stretch may change the lower bound for bifurcation during extension and inflation of cylinders. Indeed, our results show that to fully understand and capture bifurcation of extended and inflated cylinders, it is necessary to compare the mechanical properties and deformations associated with the onset of the different bifurcation modes.

In passing, we also mention that material models are mostly restricted to a limited number of phenomena and a certain time frame. In our considerations, the mechanical properties of the material have been taken to be time-independent. This assumption is reasonable when the considered time-scale is small in comparison to the typical time-scale for remodeling or viscoelastic effects. Material models that account of a deformation-dependent remodeling of the fibrous constituents have been studied in [54]. Such deformation-mediated remodeling process may be caused by external loading, but it may also be induced by swelling [32,33]. A factor that needs to be considered into account in the relation between stress and strain for the development of fibers remodeling is the maximum lifespans of the individual fibers and differences in the natural configurations of the different constituents [55, 56]. A comprehensive review on the mechano-regulated remodeling of collagen fibers has been presented in [57]. It is clear that future integration of these variables in bifurcation analyses needs the framework established in this analysis to further model aneurysms.

Our considerations take place in a membrane treatment of the cylinder, which permits analytical work in the study of geometrical instabilities. A natural extension of this work is a deeper examination of the different bifurcation modes and post-bifurcation in thick-walled cylinders, which most of the time requires the application of numerical methods. The analytical membrane analysis is a guide for the thick-walled cylinder case, which may be carried out numerically.

Author Contributions

All authors contributed equally to the final version of the article.

Acknowledgments

Not Applicable.

Conflict of Interest

The authors declare no conflict of interest.

Funding

Data Availability Statements

Not Applicable.

References

[1] Lindsay, M., Dietz, H., Lessons on the pathogenesis of aneurysm from heritable conditions, *Nature*, 473(7347), 2011, 308–31.
[2] Schermerhorn, M., A 66-year-old man with an abdominal aortic aneurysm: review of screening and treatment, *JAMA*, 302(18), 2009, 2015–2022.
[3] Corneliussen, A.H., Shield, R.T., Finite deformation of elastic membranes with application to the stability of an inflated and extended tube, *Archive for Rational Mechanics and Analysis*, 7, 1961, 273–304.
[4] Biot, M.A., *Mechanics of Incremental Deformations,* Wiley, 1965.
[5] Gonçalves, P.B., Pamplona, D.C., Lopes, S.R.X., Finite deformations of an initially stressed cylindrical shell under internal pressure, *International Journal of Mechanical Sciences*, 50(1), 2008, 92-103.
[6] Haughton D.M., Ogden, R.W., Bifurcation of inflated circular cylinders of elastic material under axial loading - I. Membrane theory for thin-walled tubes, *Journal of the Mechanics and Physics of Solids*, 27(3), 1979, 179-212.
[7] Humphrey, J.D., Eberth, J.F., Dye, W.W., Gleason, R.L., Fundamental role of axial stress in compensatory adaptations by arteries, *Journal of Biomechanics,* 42(1), 2009, 1–8.
[8] Pamplona, D.C., Gonçalves, P.B., Lopes, S.R.X., Finite deformations of cylindrical membrane under internal pressure, *International Journal of Mechanical Sciences*, 48(6), 2006, 683–696.
[9] Ogden, R.W., Incremental elastic motions superimposed on a finite deformation in the presence of an electromagnetic field, *International Journal of Non-Linear Mechanics*, 44(5), 2009, 570–580.
[10] Merodio, J., Haughton, D., Bifurcation of thick-walled cylinder shells and the mechanical response of arterial tissue affected by Marfan's syndrome, *Mechanics Research Communications*, 37(1), 2010, 1–6.

[11] Rodríguez, J., Merodio, J., A new derivation of the bifurcation conditions of inflated cylindrical membranes of elastic material under axial loading. Application to aneurysm formation, *Mechanics Research Communications*, 38(3), 2011, 203–210.

[12] Alhayani, A.A., Giraldo, J.A., Rodríguez, J., Merodio, J., Computational modelling of bulging of inflated cylindrical shells applicable to aneurysm formation and propagation in arterial wall tissue, *Finite Elements in Analysis and Design*, 73, 2013, 20–29.

[13] El Hamdaoui, M., Merodio, J., Ogden, R.W., Rodríguez, J., Finite elastic deformations of transversely isotropic circular cylindrical tubes, *International Journal of Solids and Structures*, 51(5), 2014, 1188–1196.

[14] El Hamdaoui, M., Merodio, J., Azimuthal shear of doubly fibre-reinforced, non-linearly elastic cylindrical tubes, *Journal of Engineering Mathematics*, 95, 2015, 347–357.

[15] El Hamdaoui, M., Merodio, J., Ogden, R.W., Deformation induced loss of ellipticity in an anisotropic circular cylindrical tube, *Journal of Engineering Mathematics*, 109, 2018, 31–45.

[16] Fu, Y.B., Liu, J.L., Francisco, G.S., Localized bulging in an inflated cylindrical tube of arbitrary thickness - the effect of bending stiffness, *Journal of the Mechanics and Physics of Solids*, 90, 2016, 45-60.

[17] Amabili, M., Breslavsky, I.D., Reddy, J.N., Nonlinear higher-order shell theory for incompressible biological hyperelastic materials, *Computer Methods in Applied Mechanics and Engineering*, 346, 2019, 841-861.

[18] Dehghani, H., Desena-Galarza, D., Jha, N.K., Reinoso, J., Merodio, J., Bifurcation and post-bifurcation of an inflated and extended residually-stressed circular cylindrical tube with application to aneurysms initiation and propagation in arterial wall tissue, *Finite Elements in Analysis and Design*, 161, 2019, 51–60.

[19] Font, A., Jha, N.K. Dehghani, H., Reinoso, J., Merodio, J., Modelling of residually stressed, extended and inflated cylinders with application to aneurysms, *Mechanics Research Communications*, 111, 2021, 103643.

[20] Hejazi, M., Hsiang, Y., Phani, A.S., Fate of a bulge in an inflated hyperelastic tube: theory and experiment, *Proceedings of the Royal Society A: Mathematical, Physical and Engineering Sciences*, 477, 2021, 20200837.

[21] Haughton, D., Ogden, R., Bifurcation of inflated circular cylinders of elastic material under axial loading-II. Exact theory for thick-walled tubes, *Journal of the Mechanics and Physics of Solids*, 27, 1979, 489–512.

[22] Haughton, D.M., Merodio, J., The elasticity of arterial tissue affected by Marfan's syndrome, *Mechanics Research Communications*, 36(6), 2009, 659–668.

[23] Dorfmann, L., Ogden, R.W., The effect of residual stress on the stability of a circular cylindrical tube, *Journal of Engineering Mathematics*, 127, 2021, 9.

[24] Melnikov, A., Ogden, R.W., Dorfmann, L., Merodio, J., Bifurcation analysis of elastic residually-stressed circular cylindrical tubes, *International Journal of Solids and Structures*, 226-227, 2021, 111062.

[25] Desena-Galarza, D., Dehghani, H., Jha, N.K., Reinoso, J., Merodio, J., Computational bifurcation analysis for hyperelastic residually stressed tubes under combined inflation and extension and aneurysms in arterial tissue, *Finite Elements in Analysis and Design*, 197, 2021, 103636.

[26] Barzó, P., Marmarou, A., Fatouros, P., Hayasaki, K., Corwin, F., Contribution of vasogenic and cellular edema to traumatic brain swelling measured by diffusion-weighted imaging, *Journal of Neurosurgery*, 87(6), 1997, 900-907.

[27] D'Lima, D.D., Hashimoto, S., Chen, P.C., Colwell, Jr., C.W., Lotz, M.K., Impact of mechanical trauma on matrix and cells, *Clinical Orthopaedics and Related Research*, 391, 2001, S90–S99.

[28] Tracey, K.J., The inflammatory reflex, *Nature*, 420, 2002, 853-859.

[29] Tsai, H., Pence, T.J., Kirkinis, E., Swelling induced finite strain flexure in a rectangular block of an isotropic elastic material, *Journal of Elasticity*, 75, 2004, 69–89.

[30] Zamani, V., Pence, T.J., Demirkoparan, H., Topol, H., Hyperelastic models for the swelling of soft material plugs in confined spaces, *International Journal of Non-Linear Mechanics*, 106, 2018, 297–309.

[31] Demirkoparan, H., Pence, T.J., Swelling-induced twisting and shearing in fiber composites: the effect of the base matrix mechanical response, *Emergent Materials*, 3, 2020, 87–101.

[32] Gou, K., Topol, H., Demirkoproran, H., Pence, T.J., Stress-swelling finite element modeling of cervical response with homeostatic collagen fiber distributions, *Journal of Biomechanical Engineering*, 142(8), 2020, 081002.

[33] Topol, H., Gou, K., Demirkoparan, H., Pence, T.J., Hyperelastic modeling of the combined effects of tissue swelling and deformation-related collagen renewal in fibrous soft tissue, *Biomechanics and Modeling in Mechanobiology*, 17(6), 2018, 1543–1567.

[34] Demirkoparan, H., Merodio, J., Swelling and axial propagation of bulging with application to aneurysm propagation in arteries, *Mathematics and Mechanics of Solids*, 25(7), 2020, 1459–1471.

[35] Topol, H., Al-Chlaihawi, M.J., Demirkoparan, H., Merodio, J., Bulging initiation and propagation in fiber-reinforced swellable Mooney-Rivlin membranes, *Journal of Engineering Mathematics*, 128, 2021, 8.

[36] Al-Chlaihawi, M.J., Topol, H., Demirkoparan, H., Merodio, J., On prismatic and bending bifurcations of fiber-reinforced elastic membranes under swelling with application to aortic aneurysms, *Mathematics and Mechanics of Solids*, 2022, DOI: 10.1177/10812865211058767.

[37] Chagnon, G., Rebouah, M., Favier, D., Hyperelastic energy densities for soft biological tissues: A review, *Journal of Elasticity*, 120, 2015, 129–160.

[38] Treloar, L.R.G., *The Physics of Rubber Elasticity*, Third Edition, Clarendon Press, Oxford, 1975.

[39] Demirkoparan, H., Pence, T.J., Swelling of an internally pressurized nonlinearly elastic tube with fiber reinforcing, *International Journal of Solids and Structures*, 44(11-12), 2007, 4009–4029.

[40] Demirkoparan, H., Pence, T.J., Torsional swelling of a hyperelastic tube with helically wound reinforcement, *Journal of Elasticity*, 92, 2008, 61–90.

[41] Gundiah, N., Ratcliffe, M.B., Pruitt, L.A., The biomechanics of arterial elastin. *Journal of the Mechanical Behavior of Biomedical Materials*, 2(3), 2009, 288–296.

[42] Gasser, T.C., Ogden, R.W., Holzapfel, G.A., Hyperelastic modelling of arterial layers with distributed collagen fibre orientations, *Journal of the Royal Society. Interface*, 3, 2006, 15–35.

[43] Topol, H., Jha, N.K., Demirkoparan, H., Stoffel, M., Merodio, J., Bulging of inflated membranes made of fiber reinforced materials with different natural configurations, *European Journal of Mechanics - A/Solids*, 96, 2022, 104670.

[44] Holzapfel, G.A., Gasser, T.C., Ogden, R.W., A new constitutive framework for arterial wall mechanics and a comparative study of material models, *Journal of Elasticity*, 61, 2000, 1-48.

[45] Holzapfel, G.A., Gasser, T.C., Ogden, R.W., Comparison of a multi-layer structural model for arterial walls with a Fung-type model, and issues of material stability, *Journal of Biomechanical Engineering*, 126(2), 2004, 264–275.

[46] Holzapfel, G.A., Ogden, R.W., Constitutive modelling of arteries, *Proceedings of the Royal Society A: Mathematical, Physical and Engineering Sciences*, 466, 2010, 1551-1596.

[47] Ogden, R.W., *Non-Linear Elastic Deformations*, Ellis Horwood, Chichester, 1984.

[48] Alhayani, A.A., Rodriguez, J., Merodio, J., Competition between radial expansion and axial propagation in bulging of inflated cylinders with application to aneurysms propagation in arterial wall tissue, *International Journal of Engineering Science*, 85, 2014, 74–89.

[49] Demirkoparan, H., Merodio, J., Bulging bifurcation of inflated circular cylinders of doubly fiber-reinforced hyperelastic material under axial loading and swelling, *Mathematics and Mechanics of Solids*, 22, 2017, 666–682.

[50] Qiu, G.Y., Pence, T.J., Remarks on the behavior of simple directionally reinforced incompressible nonlinearly elastic solids, *Journal of Elasticity*, 49, 1997, 1–30.

[51] Merodio, J., Ogden, R.W., Instabilities and loss of ellipticity in fiber-reinforced compressible non-linearly elastic solids under plane deformation, *International Journal of Solids and Structures*, 40(18), 2003, 4707–4727.

[52] Topol, H., Demirkoparan, H., Pence, T.J., Wineman, A., A theory for deformation dependent evolution of continuous fiber distribution applicable to collagen remodeling, *IMA Journal of Applied Mathematics*, 79(5), 2014, 947–977.

[53] Ogden, R.W., Saccomandi, G., Introducing mesoscopic information into constitutive equations for arterial walls, *Biomechanics and Modeling in Mechanobiology*, 6, 2007, 333–344.

[54] Topol, H., Demirkoparan, H., Pence, T.J., Wineman, A., Time-evolving collagen-like structural fibers in soft tissues: Biaxial loading and spherical inflation, *Mechanics of Time-Dependent Materials*, 21, 2017, 1–29.

[55] Topol, H., Demirkoparan, H., Pence, T.J., On collagen fiber morphoelasticity and homeostatic remodeling tone, *Journal of the Mechanical Behavior of Biomedical Materials*, 113, 2021, 104154.

[56] Topol, H., Demirkoparan, H., Pence, T.J., Modeling stretch-dependent collagen fiber density, *Mechanics Research Communications*, 116, 2021, 103740.

[57] Topol, H., Demirkoparan, H., Pence, T.J., Fibrillar collagen: A review of the mechanical modeling of strain mediated enzymatic turnover, *Applied*

Mechanics Reviews, 73(5), 2021, 050802.

ORCID iD

Heiko Topol https://orcid.org/0000-0002-4845-7515
Murtadha J. Al-Chlaihawi https://orcid.org/0000-0003-2036-3231
Hasan Demirkoparan https://orcid.org/0000-0003-1713-0349
José Merodio https://orcid.org/0000-0001-5602-4659

How to cite this article: Topol H., Al-Chlaihawi M.J., Demirkoparan H., Merodio J. Bifurcation of Fiber-Reinforced Cylindrical Membranes under Extension, Inflation, and Swelling, *J. Appl. Comput. Mech.*, 9(1), 2023, 113–128. https://doi.org/10.22055/jacm.2022.40949.3677

Publisher's Note Shahid Chamran University of Ahvaz remains neutral with regard to jurisdictional claims in published maps and institutional affiliations.